


PAPER



Cite this: *J. Mater. Chem. C*, 2019,
7, 8412

A flexible viscoelastic coupling cable with self-adapted electrical properties and anti-impact performance toward shapeable electronic devices†

Fang Yuan, Sheng Wang, Shuaishuai Zhang, Yu Wang, Shouhu Xuan* and Xinglong Gong *

A novel flexible cable with self-adapted electrical conductivity and anti-impact characteristics has been developed by combining the elastic PDMS shell and the viscous CNTs/STG (shear-thickening gel) string. Excitingly, the conductivity of the cable can return to the initial state while the deformation of the sensor is still maintained. Therefore, the cable exhibits rare dynamic sensitivity, which can be applied on various targets with uneven surfaces. This flexible cable shows high stretch fracture strain (151%) and its resistance is linearly dependent on the stretch strain and bending angle. The gauge factor of the cable is 1.18, which endows it with an ability to trace joints of the human body while walking, jumping and squatting. More importantly, due to the energy dissipation nature of the STG, the cable shows excellent anti-impact performance by buffering 70.5% of the impact energy and detecting high energy stimuli. An elastic-viscous combining mechanism has been proposed to discuss the mechanic–electric coupling performance, and the creep of viscous STG string plays a key role in determining the self-adapted conductivity. Because of the self-adjusting electric property, anti-impact performance, and sensing behavior, this cable can be further attached to the Kevlar fabric to form a wearable electric device to measure the distribution of pressure.

Received 12th April 2019,
Accepted 7th June 2019

DOI: 10.1039/c9tc01980d

rsc.li/materials-c

Introduction

With the development of artificial intelligence, service-oriented smart structures received considerable attention in various fields. Today, flexible electric devices are of special importance for energy regeneration,^{1,2} organic photovoltaic device assembly^{3,4} and artificial electronic skin generation^{5–9} because of their excellent stretchability and portability. Owing to the increasing demand for robots, wearable electronic devices, and medical health monitors, considerable effort has been focused on the development of highly stretchable electric devices, such as sensors, to monitor the external chemical or physical environment.^{10–15} Unlike conventional electronics, wearable sensors could be conveniently adhered to the human body for continuously monitoring the dynamic features. In consideration of the uneven surface on the joints of human body, flexible sensors

with a self-adapted shape have attracted significant research interest.

During the past decade, considerable progress on flexible sensors has been made by using diverse materials with strain dependent conductivity. Most flexible sensors comprise conductive fillers, such as silver nanoparticles/nanowires/flakes,^{16–19} conductive polymers,²⁰ carbon nanotubes^{21,22} and graphene,²³ dispersed in an insulated polymer matrix. By designing inner microstructures of conductive networks, high strain sensitivity and sensing range were achieved due to the increased spatial deformation.²⁴ Softness and deformability are attractive in wearable devices, which enable a wide range of strain deformation. Frequently, these composites were constructed from rubber,²⁵ polyurethane,^{26,27} Ecoflex,²⁸ polydimethylsiloxane (PDMS),²⁹ and polystyrene,³⁰ most of which are elastic. However, fragile textures often emerged during the installation of above devices on the uneven surface, which weakened the mechanical property and sensing behavior and thus limited their practical applications.

Plastic matrix with high viscosity showed potential in wearable sensors, electronic device, and circuit repair, due to its shapeable and self-healing properties.^{31–33} Importantly, it was found that by embedding graphene in viscoelastic polymer matrices, the plastic sensor exhibited unusual electromechanical properties.

CAS Key Laboratory of Mechanical Behavior and Design of Materials, Department of Modern Mechanics, CAS Center for Excellence in Complex System Mechanics, University of Science and Technology of China, Hefei 230027, P. R. China.
E-mail: xuansh@ustc.edu.cn, gongxl@ustc.edu.cn

† Electronic supplementary information (ESI) available. See DOI: 10.1039/c9tc01980d

The postdeformation temporal relaxation of electrical resistance and nonmonotonic changes in resistivity with strain were unprecedented due to the unique filler mobility in the viscous matrix.³⁴ Obviously, self-healing electromechanical behavior originated from the network relaxation, favorable in adapted shapeable electronic devices. By using amylopectin as the carrier, the shapeable composite with conductive green hydrogen bonded networks showed high sensing performance.³⁵ To improve the stability, a conductive MWCNT (multiwalled carbon nanotubes)–MPDMS (modified polydimethylsiloxane) nanocomposite was further developed, and it could be used in electrical circuits and flexible electronic devices due to its unique shapeable nature.³⁶ Unfortunately, it was noted that proper elasticity is necessary because of the unexpected cold-flow in the viscous sensor. Meanwhile, the combination of elastic and viscous parts delivers interesting time-dependent mechanical properties. To our knowledge, the viscoelastic coupling rheology and its further application in sensors have not been well explored.

Furthermore, in addition to the superior electrical properties, excellent mechanical properties are essentially required for

the practical application of sensors. Unfortunately, most flexible sensors exhibit low mechanical strength owing to their superior softness, and the mechanical wear over time leads to the reduction of the lifespan. The mechanical problems of sensors can be solved by improving the mechanical properties of the polymer matrix. Shear thickening gel (STG) is a viscoplastic polymer whose modulus can increase drastically under high strain rate loading by changing its physical state from liquid to solid. Owing to the unique rate-dependent characteristic, the STG can dissipate impact energy, and thus has a broad application in damping, shielding and safeguarding fields.^{37–40} The synergistic effect of wonderful STG with elastic polyurethane sponge led to higher anti-impact performance than that of the two individual components.⁴¹ Considering the self-healing, anti-impact, and time-dependent rheology of STG, designing distinct viscoelastic coupling structures for multifunctional sensing materials will be effective for applications in wearable electric devices.

In this study, we developed a novel type of a flexible cable by combining the elastic PDMS shell and the viscous conductive

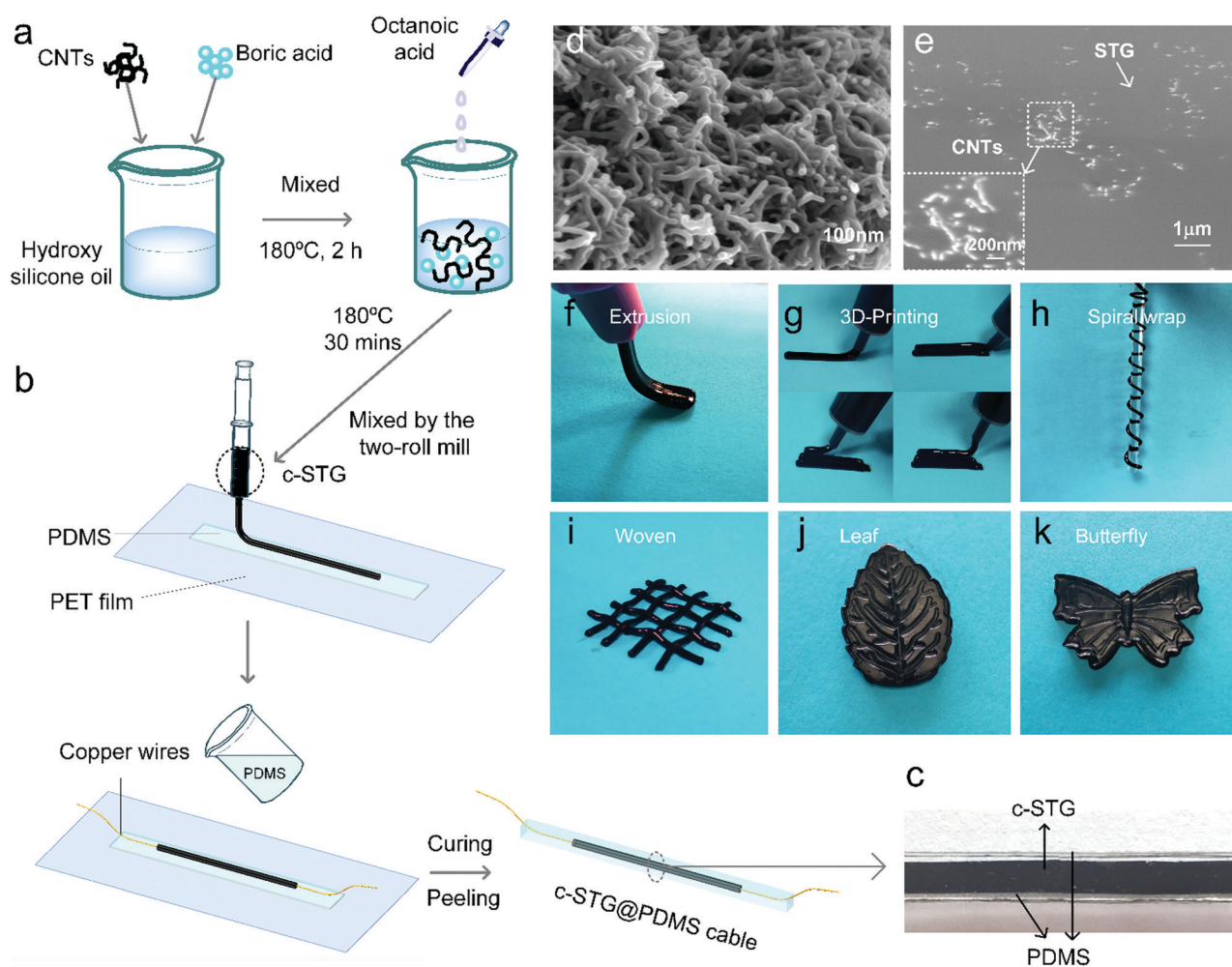


Fig. 1 The schematic illustration of the fabrication process of (a) c-STG and (b) c-STG@PDMS cable. Photograph of the c-STG@PDMS cable (c). SEM images of (d) CNTs and (e) c-STG. The c-STG can be extruded into different shapes similar to 3D-printing (f and g), spiral wrapping (h), weaving (i); c-STG were shaped by different molds (j and k).

STG (c-STG) string. The mobile c-STG was sensitive to deformation in a self-adapted time-dependent manner, while the PDMS shell endowed the cable with self-recoverability. The viscoelastic coupling behavior endowed the c-STG@PDMS sensor with high sensitivity to both static (stretch, compression, bend, and torsion) and dynamic stimuli. Besides, it could not only detect the dynamic impact from different heights but also show the safeguarding performance due to the energy dissipation of the STG. The cable could monitor the motion of the human joints of the index finger, elbow, and knee, which makes it a promising wearable electric device. Finally, the cable array could be attached to a Kevlar fabric, which allowed to detect the distribution of the applied pressure.

Results and discussion

Preparation and characterization of flexible c-STG@PDMS cable

CNTs were used as the conductive fillers in the c-STG due to their intrinsic electric conductivity. In this study, the composite materials with different mass fractions of CNTs were named c-STG composite-X, where X was the filler content. Fig. 1a and b schematically illustrate the fabrication process of the c-STG and the c-STG@PDMS cable, respectively. The obtained c-STG was extruded from a syringe in the shape of a wire and packaged using PDMS to maintain a fixed cylinder shape. Both ends of the cylinder were connected with a copper wire and a flexible c-STG@PDMS cable was obtained (Fig. 1c). Fig. 1d shows the SEM image of CNTs. It was found that these thread-like carbon nanotubes were entangled because of the wire-like nanostructure. The CNTs were uniformly dispersed after doping the CNTs into the STG matrix (Fig. 1e). The bright particles that emerged on the polymer matrix were CNTs (inset of Fig. 1e) and the smooth substrate was STG. Due to the high plasticity of the soft STG substrate, the final c-STG could be easily shaped into different structures. As shown in Fig. 1f, the c-STG can be continuously extruded from an elliptical nozzle with a flat noodle shape. Cylindrical strings were ejected from the circular nozzle, thus the c-STG showed a high potential in 3D-printing (Fig. 1g). Moreover, the extruded c-STG could wrap and adhere to a glass rod (Fig. 1h) as well as form a woven fabric (Fig. 1i). The cross section of the extrudate was dependent on the shape of the extruder nozzle. Interestingly, c-STG could be reshaped into a leaf or a butterfly with different molds (Fig. 1j and k). Therefore, c-STG potentially could be used for application in wearable and shapeable electronic devices due to its softness and moldability.

Due to the presence of conductive CNTs, the final c-STG was conductive, and its conductivity was dependent on the mass fraction of CNTs. The resistivity of c-STG decreased with the increase in the CNT content (Fig. 2a). When the mass fraction of CNTs was 0.5 wt%, the resistivity of c-STG was $1.72 \times 10^8 \Omega \text{ m}$. However, if the CNT content increased to 1 wt%, the resistivity drastically decreased to $1.87 \times 10^3 \Omega \text{ m}$. Besides, when the mass fraction of CNTs further increased to 2%, 3%, and 4%, the

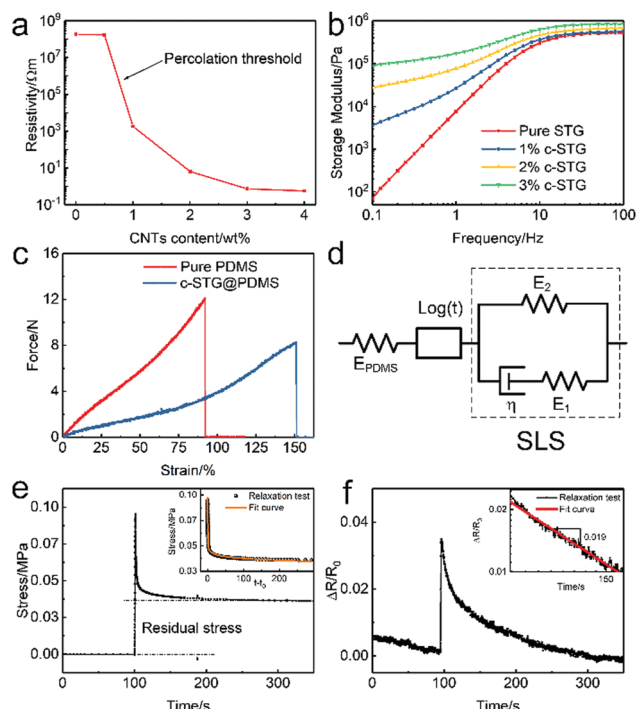


Fig. 2 (a) Resistivity as a function of CNT content of c-STG; Rheological properties of the c-STG@PDMS cable: (b) the storage modulus of STG with different mass ratios of CNTs, 0 wt%, 1 wt%, 2 wt%, and 3 wt%; (c) the stretch force–strain curves of the c-STG@PDMS cable and PDMS; (d) extended standard linear solid model with an element produced by the logarithmic creep of CNTs and a spring by PDMS; (e and f) mechanical and electrical relaxation of the c-STG@PDMS cable under 10% compressive strain.

resistivity decreased to $6.43 \Omega \text{ m}$, $0.72 \Omega \text{ m}$ and $0.56 \Omega \text{ m}$, respectively. As shown in Fig. 2a, the percolation threshold of c-STG was between 0.5 wt% and 1 wt%, and the resistivity of c-STG was stable above 2 wt%. In this study, the high conductivity of c-STG was very important, so the c-STG with 2 wt% CNTs was chosen as the optimum sample for the following preparation of the c-STG@PDMS cable.

Owing to the rate-dependent characteristic inherited from the STG, the c-STG also exhibited a typical shear thickening behavior (Fig. 2b). For the pure STG, when the shear frequency was kept at 0.1 Hz, the initial storage modulus (G_{min}') was low (67 Pa), presenting a soft viscosity state. As soon as the shear frequency reached 100 Hz, the maximum storage modulus (G_{max}') increased by 4 orders of magnitude ($5.2 \times 10^5 \text{ Pa}$), exhibiting the typical shear thickening (ST) effect. Here, due to the particle-strengthening effect⁴² of CNTs, c-STG became stiffer than STG; thus, G_{min}' of c-STG-1% increased to 3579 Pa. G' and G'' increased with the increasing CNT content in c-STG. In the meantime, the loss coefficient δ of c-STG decreased compared to those of the pure STG (Fig. S1, ESI†), indicating that the incorporation of CNTs strengthened the mechanical properties of STG and prevented the cold-flow phenomenon to a certain degree.⁴³ However, the c-STG still exhibited the cold-flow behavior under gravity, and its shape could not be maintained for a long time.

In this study, the elastic PDMS layer covered the c-STG and the c-STG@PDMS viscoelastic coupling cable was obtained. Fig. 2c depicts the force–strain curve of the c-STG@PDMS, indicating that the cable exhibits good stretchability. The fracture strain of the cable and the PDMS was 151% and 92%, respectively.

Compared to the pure PDMS, the c-STG@PDMS cable exhibited better malleability. A sustaining compression strain was applied to the c-STG@PDMS cable to investigate the self-adapted properties, and the experiment was carried out *via* a loading–holding process. The resistance and the pressure of the cable increased immediately under the strain. Here, the equation

$$\Delta R/R_0 = (R - R_0)/R_0 \quad (1)$$

defined the relative resistance change to characterize the mechano-electrical properties. During the holding process, the stress instantaneously decreased from 0.955 MPa to 0.375 MPa and the resistance kept decreasing with time, eventually recovering back to the initial value (Fig. 2e and f). In addition to the improved mechanical properties, this c-STG@PDMS viscoelastic coupling cable exhibited an exciting self-adapted conductivity.

Both the mechanical and electrical properties of the c-STG@PDMS cable were critical for its practical application. The standard linear solid (SLS) model is favorable to describe the viscoelastic behavior^{34,44} and the logarithmic creep⁴⁵ was found in the relaxation test of CNTs. Therefore, in order to

understand the mechanical and electrical relaxation, an extended SLS model simultaneously taking into account the elasticity of the PDMS shell and the influence of CNTs was proposed (Fig. 2d). According to Rod Cross,⁴⁴ the force of STG under constant compression is determined by

$$F = (E_2 + E_1 e^{-t/\tau})x, \quad (2)$$

where E_1 and E_2 are the elastic moduli which are related with the G' and G'' of c-STG,³⁴ respectively, $\tau = \eta/E_1$, η is the viscosity, and x is the constant compression displacement. By adding a logarithmic term, the stress of the c-STG@PDMS cable was obtained by the following equation.

$$\sigma = Ae^{-t/\tau} + B \log(t) + C \quad (3)$$

The first exponential term represents the time-dependent viscoelastic influence of STG. The second term was produced by the logarithmic creep of CNTs. The last constant corresponded to the elastic part. A , B , and C are associated with the structure of the cable. The stress relaxation data was fitted well using eqn (2). On the other hand, the resistance which was in accordance with result of Boland's theory.³⁴

$$\Delta R/R_0 \propto t^{-n} \quad (4)$$

As shown in Fig. 2f, the exponent n was approximately -0.019 in this study. When the compression strain was applied, the c-STG@PDMS cable was squished. Due to the plastic characteristic of the STG, the loading force decayed quickly and the elastic PDMS

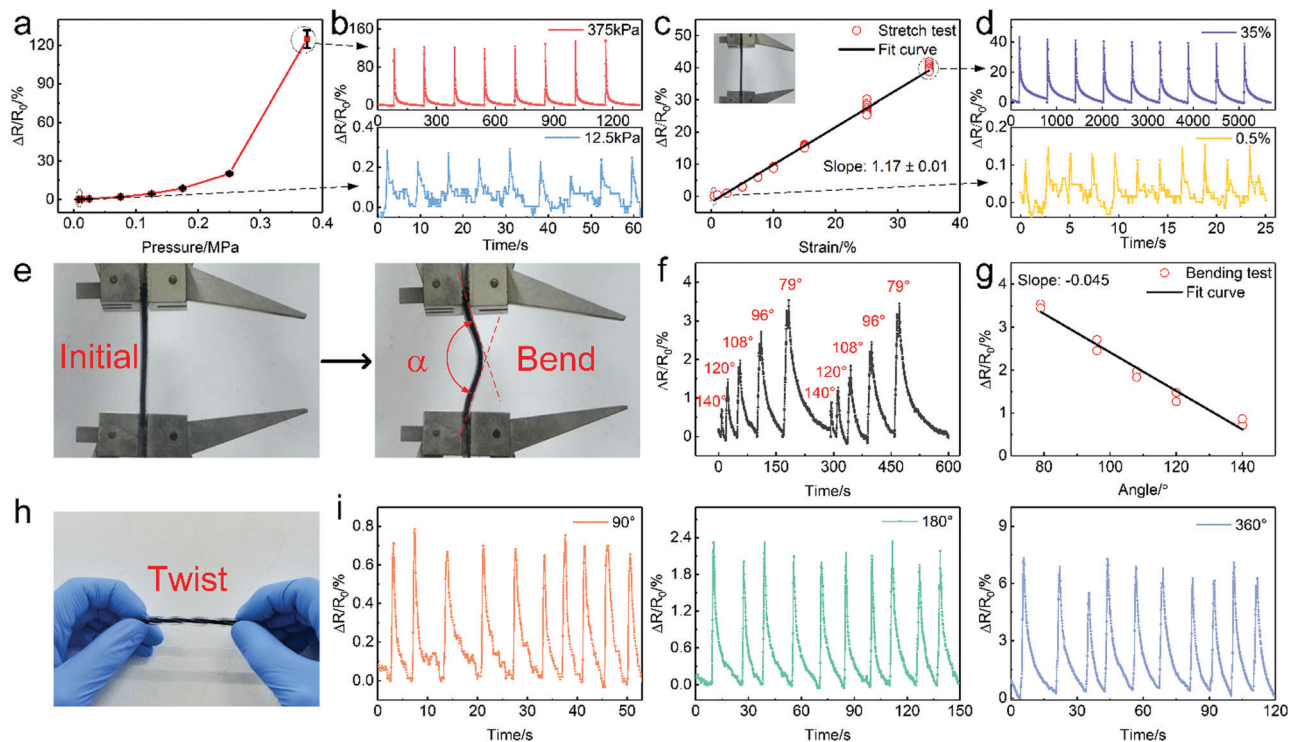


Fig. 3 (a) The resistance changes vs. the applied pressure and (b) the cycling performance under 375 kPa and 12.5 kPa. (c) The linear fitting plot of the electrical response to stretch stimuli and (d) the results of 0.5% and 35% stretch strains. (e) Bending test with MTS, (f) the resistance response to different bending angles, and (g) the fitting curve of $\Delta R/R_0$ vs. bending angle. (h) Photo of the twisting test and (i) the relative resistance change during the cyclic twist tests with different twisting angles.

shell contributed to the residual force. The soft STG relaxed easily, causing a drastic decrease in the force. The elastic PDMS caused the residual stress under compression. After unloading, the elastic PDMS forced the c-STG to take the initial shape and its conductivity re-covered.

Static mechano-electrical performance of the c-STG@PDMS cable

The static mechano-electrical performance of the c-STG@PDMS cable under the external stimuli (compression and stretch) was systematically investigated (Fig. 3a–d). Under external stimuli, the resistance of the c-STG@PDMS, which originated from the c-STG, increased due to the breakage of the conductive net. As shown in Fig. 3a, the relative resistance change in the c-STG@PDMS cable varied with the applied compression, and the peak value of $\Delta R/R_0$ increased with the increasing pressure. The cyclic tests conducted under the highest pressure (375 kPa) and very low pressure (12.5 kPa) are shown in Fig. 3b. The resistance increased as the pressure was applied and decreased with the unloading process. During the loading–unloading cycles, the cable showed excellent sensitivity and steady response to external stimuli. Meanwhile, $\Delta R/R_0$ of the cable presented a nearly linear dependency on the stretch strain amplitude when the strain was relatively low (Fig. 3c). The gauge factor ($g = \Delta R/R_0/\epsilon$) of the stretch experiment was around 1.18. Besides, the same tests were conducted with the c-STG-1%, and the strain rate showed the same effect on the gauge factor when the strain rate of the stimuli was below the critical rate of the shear thickening (Fig. S2 and S3, ESI†). The cyclic sensing performance with a stretch of 35% and 0.5% is displayed in Fig. 3d, indicating that the c-STG@PDMS cable possessed mechano-electrical stability.

Similarly, the electrical properties of the c-STG@PDMS cable during the bending test were studied. The bending angle was defined as shown in Fig. 3e. Resistance increased during the loading process and recovered to the initial value after unloading. The peak value of $\Delta R/R_0$ increased with the decrease in the bending angle (Fig. 3f). When the bending angle decreased from 140° to 79° , the peak value of $\Delta R/R_0$ increased from 0.71% to 3.54%, respectively. The fitting curve of $\Delta R/R_0$ vs. the bending angle (Fig. 3g) revealed that $\Delta R/R_0$ was almost linearly dependent on the bending angle. The electrical response of the c-STG@PDMS cable at different twist degrees was also explored (Fig. 3h and i). As the torsion angle varied from 90° to 180° to 360° , the peak values of $\Delta R/R_0$ increased from 0.75% to 2.2% to 7.5%, respectively. During the loading and unloading cycle, the sample showed a stable and repeatable response to torsion. Therefore, the c-STG@PDMS cable exhibited excellent mechano-electrical performance under various conditions and could be further used as a sensor to detect the external static stimuli.

The dynamic mechano-electrical properties and the safeguarding performance of the c-STG@PDMS cable under impact

Due to the rate-dependent shear thickening characteristic of the c-STG, the electrical and mechanical properties of the

c-STG@PDMS cable exhibited a unique response to the dynamic impact. The impact test was performed on the cable by using the drop hammer machine with a 0.24 kg impactor. The falling height varied from 5 to 20 cm. The cable was fixed on the force transducer, which was further placed on the bottom of a metal pedestal. As a comparison, pure PDMS (curing agent ratio 10:1) specimens (the same size as the c-STG@PDMS cable) and the metal pedestal without specimens were both tested. During the impact, the force signals were captured by the force transducer and recorded using an oscilloscope. The electrical data were simultaneously saved by electrical impedance spectroscopy (EIS) system. The fall height of the impactor varied from 5 cm to 20 cm, and the peak value of $\Delta R/R_0$ increased from 558% to 1438%, respectively. The increase in the drop height led to the rise of $\Delta R/R_0$ (Fig. 4a). According to Boland's theory,³⁴

$$\Delta R/R_0 \propto (E_{mgh})^k, \quad (5)$$

where the impact energy E_{mgh} ($E_{mgh} = mgh$) is proportional to the drop mass (m) and drop height (h) and k is a constant, dependent on the conductive polymer characteristics. After fitting the data (Fig. 4b), it was found that $k = 0.64$ in this case.

Fig. 4c–f shows the force response to drop hammer impact (0.24 kg) exerted from different heights. As the drop hammer struck the force transducer, the impact force started to increase to the maximum value and attenuated to 0 before the hammer bounced back. Apparently, the higher impact energy led to the

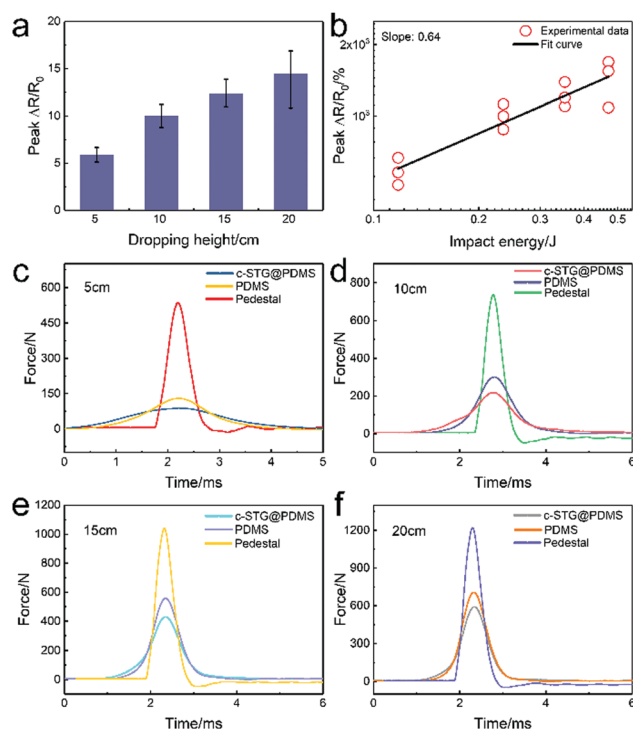


Fig. 4 Dynamic stimuli sensing performance: (a) electrical sensing response versus dropping height and (b) the fitting curve of peak $\Delta R/R_0$ versus impact energy. (c–f) Impact energy dissipation behavior of tubular cable compared to that of PDMS and metal pedestal at 5–20 cm.

larger force transmitted to the force transducer. Therefore, more damage was caused to the conductive network inside the c-STG, leading to an increase in the peak $\Delta R/R_0$ value (Fig. 4a and b).

Keeping the height at 10 cm (Fig. 4d), as soon as the drop hammer struck the rare force sensor, the loading force increased to the maximum value (737.4 N) and decayed to 0 within 0.5 ms. However, the maximum force of PDMS (299.7 N) was only 40.6% of the pedestal (737.4 N). The same phenomena were demonstrated for other heights (Fig. 4c–f). Thus, PDMS was capable of buffering the impact force. More importantly, the peak force of the c-STG@PDMS cable was further decreased to 217 N, which was reduced by 70.5% compared to that of the metal pedestal (737.4 N). Clearly, the c-STG@PDMS cable showed the best energy adsorption. Owing to the STG property, the cable offered the optimal buffering effect by absorbing most of the impact energy. In conclusion, the cable not only showed anti-impact properties but also monitored the number of impacts.

Self-adapted sensing and self-healing performance of the c-STG@PDMS cable

Due to the plastic characteristic, STG could adjust its state to external conditions and showed self-healing during its application. After coating with PDMS, the final c-STG@PDMS cable displayed unique viscoelastic coupling behavior and mechano-electrical properties, exhibiting high potential for wearable sensor applications. In this study, the self-adapted resistance and self-healing properties of the c-STG@PDMS cable were explored.

Firstly, the cyclic bending–holding–unloading experiment was carried out to investigate the self-adapted sensing behavior of the c-STG@PDMS cable. Different from the previously reported elastic sensors, the c-STG@PDMS cable can sense the external stimuli as soon as the loading occurs, while its resistance decays to the initial state under a sustained bending deformation. This type of special self-adapted resistance was studied by conducting the bending–holding–unloading experiment with the bending angles varying from 140° to 79°. As shown in Fig. 5a, the resistance varied over time during the bending–holding–releasing process under different bending angles.

The resistance reached its peak value after the loading and then decreased to the initial value during the holding process. After releasing the bending deformation, the resistance increased first and finally returned to the original value. The resistance decreased during the holding process in both compression and bending experiments. This phenomenon indicated that the flexible cable could automatically adjust its resistance to the initial value under the sustained pressure and bend. Interestingly, the resistance increased both at the initial and the final loading. This response was similar to that of the rapidly adapting receptors in human skin.^{46,47} Thus, due to the unique rapid adapting property, the cable showed the potential application in artificial human skin and robots. Moreover, the trend of peak values of the $\Delta R/R_0$ with different bending angles

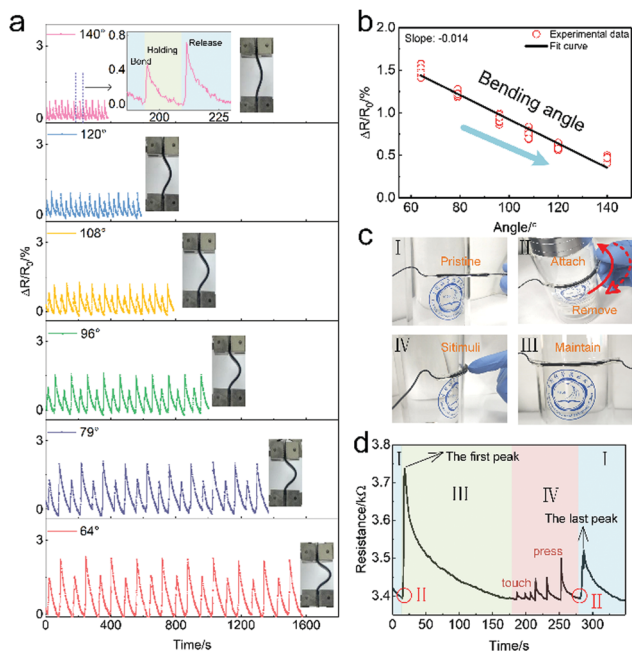


Fig. 5 (a) $\Delta R/R_0$ at different bending angles during the bending–holding–releasing process, (b) variation of $\Delta R/R_0$ as a function of bending angle during the bending process, (c) the sensing performance after sticking to the curved surface of a cup and (d) the electrical resistance change at different stages.

was similar to that in the previous bending experiment, showing an approximately linear relationship with the bending angle (Fig. 5b).

To further investigate the resistance recovery performance of the c-STG@PDMS cable, the sensing test was conducted on a curved surface, such as a cup. The cable was lying flat at first (Fig. 5c-i), and the electric signals were stable at about 3400 Ω . Then, the cable was attached to the curved surface of the cup (Fig. 5c-ii) and the resistance increased when the cable began to bend. Then, the resistance decreased after the cable was attached to the cup (Fig. 5c-iii). The recovery time for the resistance to 3400 Ω was 140 s, which indicated that the tubular sensor could adjust itself to the curve surface very quickly. Finally, the resistance of the cable was stable and the cable could detect gentle touch and press (Fig. 5c-iv), exhibiting excellent sensing performance after the self-adaptation process. Moreover, when the cable was removed from the surface of the cup (Fig. 5c-ii), the resistance first increased and then decreased to its initial value (Fig. 5c-i), showing a good recycling property. The first and the last peak of resistance were caused by the movement while attaching and removing the cable. Actually, this unusual sensing property originates from the plastic nature of the c-STG, which will be widely applied in the irregular and complicated structure with an uneven surface. The wonderful cyclability also enables its promising application in the detection of the external stimuli due to self-adapted electric properties.

Due to the gel-like characteristic of the STG, the c-STG@PDMS cable exhibited electrical self-healing. A demonstrative experiment was conducted with a closed loop circuit, including an LED bulb, a

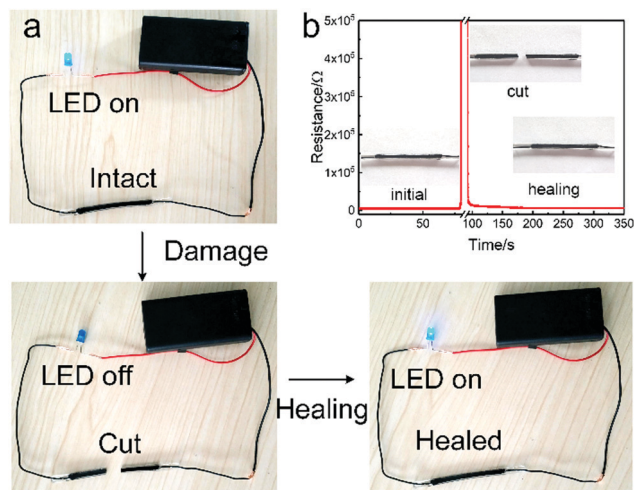


Fig. 6 (a) Digital photographs of the healing process for a conductive tubular cable in series with an LED and a battery; (b) time evolution of the electrical healing process by reattaching the cables at room temperature.

cell, and conductive wires (Fig. 6a). The LED bulb lighted up when an intact c-STG@PDMS cable was connected to the circuit. As the cable was cut off, the LED bulb extinguished because of the open circuit. Interestingly, the LED bulb lighted up again after the cut section of the cable was reattached. The real-time electrical signal of this cut-heal process was recorded (Fig. 6b). During the self-healing process, the resistance of the circuit quickly returned to its initial state, which clearly demonstrated the self-healing electrical property of the c-STG@PDMS cable. In this case, because the c-STG was viscoelastic, the self-healing electrical behavior may have been induced by mechanical self-healing. Once the cut cable sections were put together, they reconnected due to the plastic STG, and thus a loop circuit was formed again. The mechanical and electrical self-healing characteristics endowed the c-STG@PDMS cable with recycling ability and a longer lifespan.

Mechano-electrical coupling mechanism of the c-STG@PDMS cable

In this study, the c-STG@PDMS cable was found to exhibit a special viscoelastic coupling mechanical behavior. Thus, it

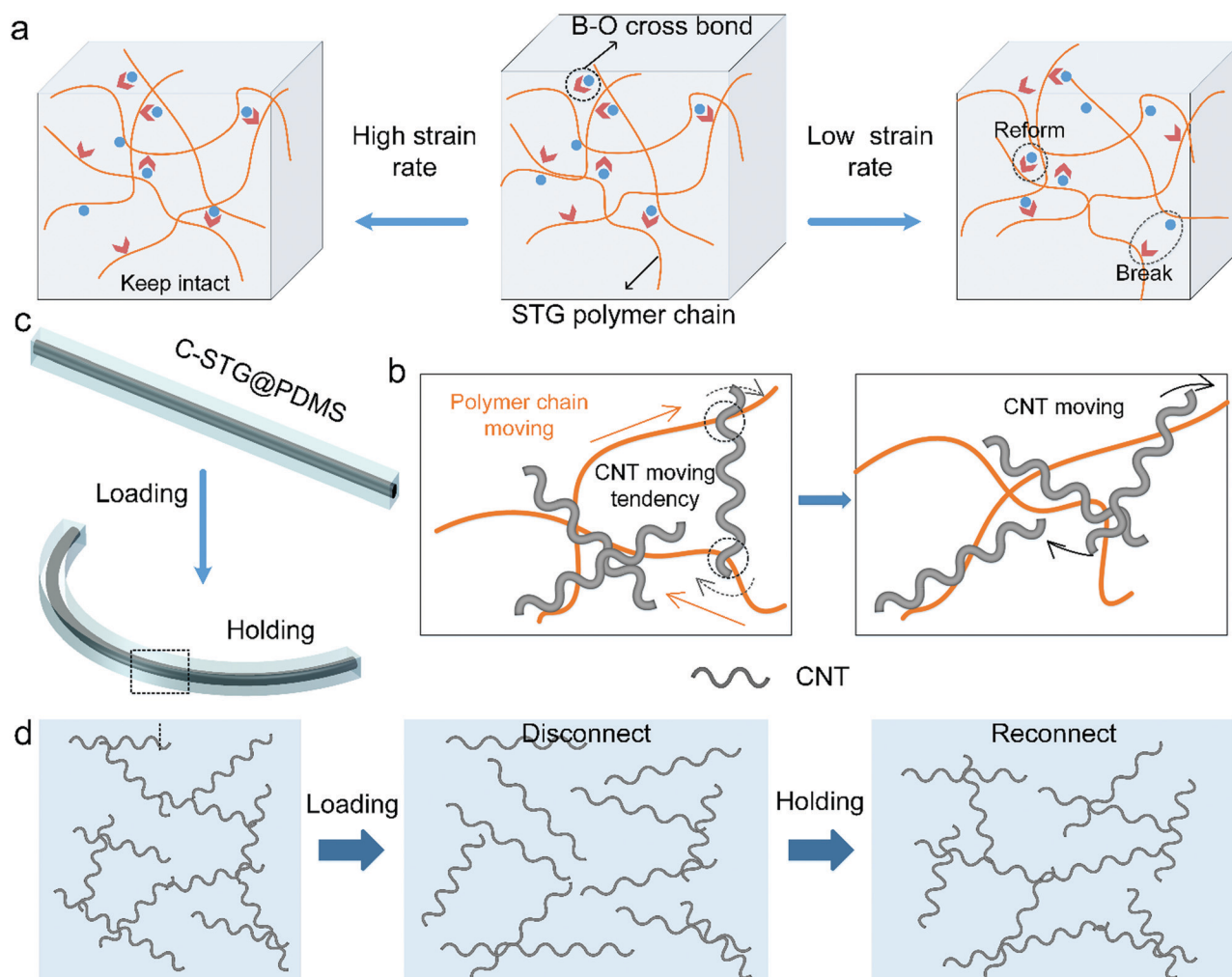


Fig. 7 (a) Mechanism of the rate-dependent behavior of the STG, (b) the movement of the CNTs inside the STG varied with the movement of the polymer chains, (c) the c-STG@PDMS cable during the loading-holding process and (d) conductive network under external stimuli.

exhibited a unique mechano-electrical sensing ability, self-adapted resistance, mechanical self-healing property, and anti-impact performance. A schematic illustration depicting the mechanism of the mechano-electrical coupling sensing behavior of the c-STG@PDMS cable is presented in Fig. 7a. Similar to the previous report,⁴¹ owing to the electron-deficient p orbital of the B atoms and redundant electrons in the orbital of O atoms, dynamic B–O cross bonds were formed in STG with rate-dependent mechanical characteristic. Because the cross bonds were transient and dynamically variable, weaker than the covalent bonds, a three-dimensional network was formed in the STG by connecting the polymer molecular chains *via* these cross bonds. At a low strain rate, these cross bonds relaxed and disconnected easily, and the relatively stable three-dimensional network disentangled to mobile molecular chains, exhibiting internal mobility. In this case, the STG was soft and plastic with a low storage modulus. However, under high strain rate, the cross bonds could not adjust to the fast dynamic strain rate in time. The disentanglement of the network was unable to keep pace with the strain rate, so the cross bonds caused a significant increment in the storage modulus.

The transformation from the plastic to the solid state exhibited the shear thickening effect. In this study, the c-STG also exhibited the typical shear thickening behavior, and the initial storage modulus of the c-STG was increased due to the presence of CNTs. The c-STG exhibited a typical plastic behavior; thus, it could not return to its initial state after deformation. Once the c-STG@PDMS cable was deformed, the soft inner c-STG was forced back to the initial state by the immediate resilience of the outer elastic PDMS. Therefore, the c-STG@PDMS cable possessed both shear thickening and viscoelastic coupling properties.

Besides increasing the stiffness, the CNTs in the STG also provided the mechano-electrical property because they could form conductive networks in the polymer matrix. When the gap between conductive CNTs was small, the quantum tunneling effect occurred and the c-STG became conductive. The change in the electrical resistance was mainly controlled by three factors: the gaps between conductive fillers, the evolution of the conductive paths, and the tendency of fillers to move.^{48,49} Respectively, the decrease in the gaps, the reformation of the conductive paths, and the incorporation of individual fillers into the conductive paths contributed to the decrement of electrical resistance. On the contrary, the resistance increased due to the destruction of the conductive paths. When the loading rate was low, the c-STG was plastic, and hence the polymer molecular chains moved easily, driving the movement of CNTs (Fig. 7b) to form the conductive network. Thus, the electrical resistance recovered with the formation of the conductive network. Besides, the electrical resistance of the c-STG@PDMS cable increased with the deformation because the three-dimensional conductive network was destroyed during the loading (such as bending, stretching, pressing, and twisting). After the loadings were released, the conductive network reformed and then the resistance decreased with time. Moreover, further deformation led to additional destruction of the

conductive network, and the peak value of $\Delta R/R_0$ simultaneously increased.

The self-adapted phenomenon of the c-STG@PDMS cable, of which the resistance decreased under sustaining loading, was responsible for resistance relaxation (Fig. 7c and d).⁵⁰ In the bending–holding–releasing experiment, different bending angles were applied to the c-STG@PDMS cable and the resistance dropped during the holding process. Owing to the plasticity of STG, the polymer segments kept moving under fixed loading, and the CNTs moved with the movement of the polymer molecular chains.^{50,51} The conductive paths were reconstructed gradually with the movement of the polymer segments, leading to decreased resistance (Fig. 7d). Therefore, the resistance decreased as the c-STG in the c-STG@PDMS cable relaxed. Then, the cable was released to return to its original state, and the resistance increased to another peak value again. The unloading process as well as the loading process were sudden macroscopic deformations, which caused sudden breaks in the conductive paths, leading to the “rapid adapting” behavior. In conclusion, the formation effect was dominant during the holding and post-releasing period, decreasing the resistance. The destruction effect played the leading role during the bending and pre-releasing period, increasing the resistance.

Different from the previous polymer-based sensors, the c-STG possessed the typical energy adsorption advantage; thus, it had a dynamic impact. Under the high rate or energy impact, the c-STG in the c-STG@PDMS cable transformed from gel to elastic state, and this change caused a sharp increase in the resistance. The relative $\Delta R/R_0$ value increased with the impact. Thus, the c-STG@PDMS cable could be further used for detecting the dynamic impact. After the impact was unloaded, the c-STG re-covered to the initial state by both gel relaxing and PDMS confining. Moreover, the self-healing characteristic of the c-STG@PDMS cable must be addressed for the formation of the dynamic B–O cross bonds in the c-STG. After re-connecting the cut c-STG@PDMS cable, the two compatible parts were bonded together and numerous new B–O cross bonds were formed simultaneously. During the following relaxing process, CNTs of the broken conductive networks start to bridge together owing to the movement of polymer molecular chains. Finally, the electrical resistance returned to the initial state.

Applications of the c-STG@PDMS cable

The flexible c-STG@PDMS cable was able to detect various stimuli with high sensitivity and stability. Therefore, it could be attached to the human body as a wearable sensor to monitor the human body motions. The cable was attached to different joints of the human body, such as the finger, elbow, and knee. The cable was attached to the external surface of the index finger (Fig. 8a), and the change in the electric signals corresponding to the different movements was recorded (Fig. 8c). As the index finger moved from *I* to *V*, $\Delta R/R_0$ changed from 1.05% to 14.02%. When the monitoring target was changed to the elbow, the bending angle changed (Fig. 8b). Clearly, the trend for the change of $\Delta R/R_0$ was similar to that of the index finger.

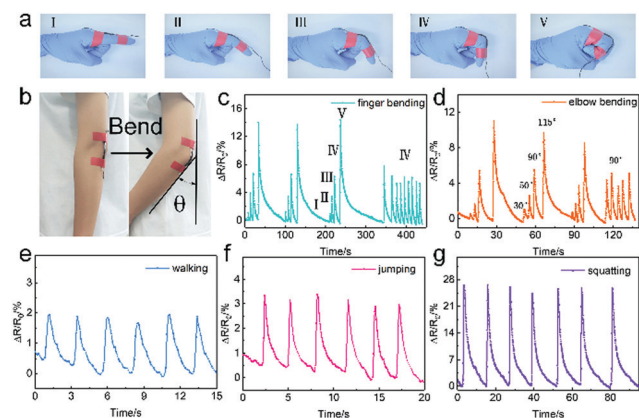


Fig. 8 Human motions monitored by c-STG@PDMS cable: (a and b) photos of the c-STG@PDMS cable attached to the index finger and the elbow and (c and d) corresponding $\Delta R/R_0$ changes; (e–g) $\Delta R/R_0$ changes during walking, jumping and squatting.

When the elbow bending angle was varied from 30° to 115° , the peak value of $\Delta R/R_0$ increased from 0.76% to 9.74% (Fig. 8d). The motions of the knee, such as walking, jumping and squatting, were also investigated by attaching the cable to the knee (Fig. 8e–g). The peak value of $\Delta R/R_0$ for the different movements such as walking, jumping and squatting was 2.0%, 3.4%, 27.8%, respectively. The different electric responses of the human motions demonstrated the high sensitivity and the stable output signals of under repeated cycling deformations suggested the reliability and stability. Based on the above analysis, it can be concluded that the c-STG@PDMS cable exhibited a promising potential in wearable electrical devices for human motion detection.

As the inner part of the c-STG@PDMS cable was adhesive and could be molded easily at a low loading rate, it could be attached to a fabric as a wearable electric device. For example, four linear c-STG strings were placed on the surface of Kevlar fabric end to end, forming a square closed loop, and four copper wires were inserted into the four vertices of the c-STG square. A thin layer of PDMS covered the surface. As shown in Fig. 9a and c, the c-STG square loop was sealed between Kevlar fabric and PDMS. The obtained Kevlar-c-STG-PDMS was tested *via* the electric signal output of four copper wires when pressure was applied to different positions, including vertices and the middle of the sides of the c-STG square. Here, the resistance of one c-STG side and vertex under pressure were studied. Fig. 9b shows the schematic illustration of the circuit of the square loop structure inside the Kevlar-c-STG-PDMS. The resistance between A and B was defined as R_{AB} and the definitions of the rest were similar. Once a force of 0.3 N was applied to point A by MTS, R_{AB} and R_{DA} increased compared to R_{BC} and R_{CD} (Fig. 9e). Similarly, when the same force was applied to the medium of the line AB, only R_{AB} showed a relative increase (Fig. 9f). This result indicated that the array structure was capable of detecting the loading position and could be used as a wearable electrical skin device. Since the c-STG could be easily adhered to the fabric and encapsulated by PDMS, this

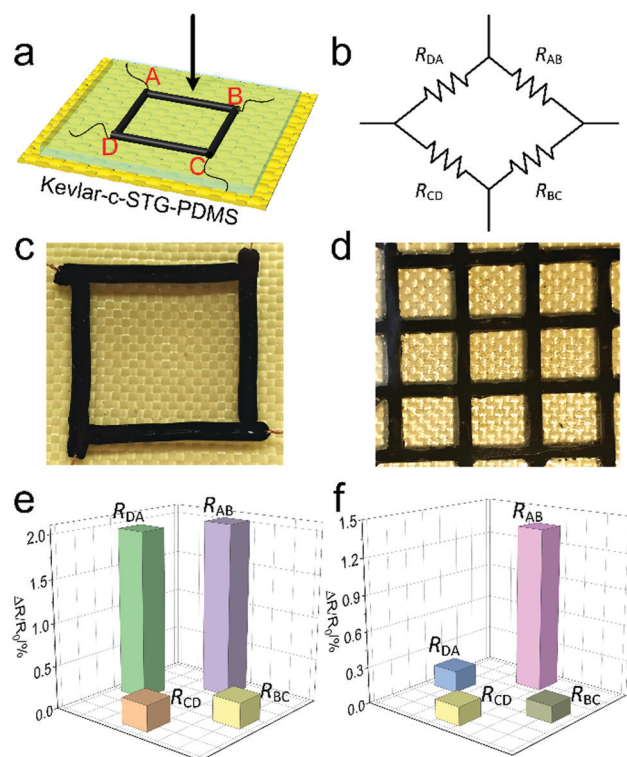


Fig. 9 (a) Schematic illustration of Kevlar-c-STG-PDMS and (b) the circuit of the composite; (c) a digital photograph of the Kevlar-c-STG-PDMS and (d) the array composite; distribution of the resistance of the Kevlar-c-STG-PDMS composite under pressure at different positions, (e) corresponding to the pressure from A point, (f) corresponding to the pressure along line AB.

c-STG arrays on the Kevlar fabric can be varied by changing the distribution of the c-STG string, as shown in Fig. 9d. As a result, the c-STG-PDMS shows potential in forming different structures and exhibits broad applications in wearable electric sensors.

Experimental

Materials

Hydroxyl silicone oil and boric acid were purchased from Sinopharm Chemical Reagent Co. Ltd, Shanghai, China. CNTs with a diameter of 8–15 nm and length of 3–12 μm were provided by Conductive Materials of Lueldia Co. Ltd, Xinxiang City, Henan Province, China. The PDMS precursor and the curing agent (Sylgard 184) were purchased from Dow Corning GmbH, USA. All chemical reagents were of analytical purity and used as received without further purification.

Fabrication of c-STG

Hydroxyl silicone oil and boric acid with a weight ratio of 20 : 1 and varying amounts of CNTs were vigorously stirred to yield a homogeneous mixture. After heating in a 180°C oven for 90 min, few drops of octanoic acid were added. Then, the mixture was stirred and heated at 180°C for another 30 min. After cooling to room temperature, the mixture was homogenized by the two-roll mill (Taihu Rubber Machinery Inc., China, model XK-160).

Preparation of c-STG@PDMS

Firstly, the precursor and the curing agent of PDMS (Dow Corning GmbH, USA) were mixed in a 10:1 weight ratio. A thin layer of the uniform mixture was cured in an oven at 90 °C for 5 min. Secondly, the linear shape of c-STG was extruded by using a syringe. The c-STG string was paved on the PDMS substrate and both sides were connected with copper wires. After this “printing process”, the PDMS mixture was poured onto the c-STG string. Then, the as-prepared sample was heated at 90 °C for 15 min. After the PDMS was completely cured, the linear c-STG string encapsulated by PDMS and a cable-like product was obtained. The Kevlar-c-STG-PDMS sample was fabricated in a similar way. The bottom PDMS substrate was replaced with the Kevlar. Besides, the inner c-STG turned into four strings connected end to end and every junction was connected with a copper wire.

Characterization

The morphology of CNTs and c-STG was characterized by field emission scanning electron microscopy (FE-SEM, XL30 ESEM). The rheological properties of STG and c-STG were tested by a commercial rheometer (Physica MCR 302, Anton Paar Co., Austria). Cylindrical samples with a thickness of 1 mm and a diameter of 20 mm were tested between a parallel plate (diameter: 20 mm) with the shear frequency exponentially increasing from 0.1 Hz to 100 Hz and the strain amplitude was set at 0.1%. The static stimuli experiment (stretching, compressing, and bending) was conducted on a universal test machine (MTS criterion 43, MTS System Co., America). The electrochemical impedance spectra (EIS) system, including modulab material test systems, data storage, and an analysis system, were simultaneously utilized to test and record the electrical data. The dynamic impact test was performed using a drop hammer test device (ZCJ1302-A, MTS System Co., America) equipped with a force sensor and a data acquisition system.

Conclusions

In this study, a flexible wearable c-STG@PDMS cable with self-adapted properties was developed by wrapping the c-STG string with a PDMS shell. The cable exhibited excellent sensing performance and a steady response to static stimuli, such as bending, twisting, stretching and pressing deformations. On the other hand, owing to the ST property of the inner c-STG, the cable could respond to dynamic impact stimuli and buffer the impact force by approximately 70%, indicating that the cable could be utilized as a sensor with safeguarding performance. More importantly, the cable exhibited the self-adapted electrical capability. As a novel visco-elastic coupling sensor, it can adjust itself to the external environment when attached to an uneven surface. In our experiment, the c-STG@PDMS cable showed stable and repeatable responses to finger and elbow bending at different angles and the movement of the legs (walking, jumping and squatting). This flexible cable with high sensitivity could be further applied in wearable devices to monitor body motions and

simultaneously detect external stimuli. Besides, the Kevlar-c-STG-PDMS composite showed excellent sensing performance by detecting the distribution of external stimuli. Finally, it was found that this type of soft sensor has broad potential in the coming-generation wearable electric devices.

Conflicts of interest

There are no conflicts to declare.

Acknowledgements

Financial support from the National Natural Science Foundation of China (Grant No. 11822209, 11772320), the Strategic Priority Research Program of the Chinese Academy of Sciences (Grant No. XDB22040502), and the Fundamental Research Funds for the Central Universities (WK2090050045) is gratefully acknowledged. This study was also supported by the Collaborative Innovation Center of Suzhou Nano Science and Technology.

References

- 1 T. J. Trivedi, D. Bhattacharjya, J. S. Yu and A. Kumar, *ChemSusChem*, 2015, **8**, 3294–3303.
- 2 H. Deng, Y. Du, Z. Wang, J. Ye, J. Zhang, M. Ma and X. Zhong, *Commun. Phys.*, 2019, **2**, 21.
- 3 R. Arai, S. Furukawa, Y. Hidaka, H. Komiyama and T. Yasuda, *ACS Appl. Mater. Interfaces*, 2019, DOI: 10.1021/acsami.9b00018.
- 4 Z. Y. Yin, S. Y. Sun, T. Salim, S. X. Wu, X. A. Huang, Q. Y. He, Y. M. Lam and H. Zhang, *ACS Nano*, 2010, **4**, 5263–5268.
- 5 X. Wang, Y. Gu, Z. Xiong, Z. Cui and T. Zhang, *Adv. Mater.*, 2014, **26**, 1336–1342.
- 6 M. Li, Y. Wang, Y. Zhang, H. Zhou, Z. Huang and D. Li, *J. Mater. Chem. C*, 2018, **6**, 5877–5887.
- 7 S. Wang, L. Gong, Z. Shang, L. Ding, G. Yin, W. Jiang, X. Gong and S. Xuan, *Adv. Funct. Mater.*, 2018, **18**, 1707538.
- 8 Y. Fu, H. He, Y. Liu, Q. Wang, L. Xing and X. Xue, *J. Mater. Chem. C*, 2017, **5**, 1231–1239.
- 9 I. You, S.-E. Choi, H. Hwang, S. W. Han, J. W. Kim and U. Jeong, *Adv. Funct. Mater.*, 2018, **28**, 1801858.
- 10 B. Liang, W. Chen, Z. He, R. Yang, Z. Lin, H. Du, Y. Shang, A. Cao, Z. Tang and X. Gui, *Small*, 2017, **13**, 1702422.
- 11 J. Lee, M. Lim, J. Yoon, M. S. Kim, B. Choi, D. M. Kim, D. H. Kim, I. Park and S. J. Choi, *ACS Appl. Mater. Interfaces*, 2017, **9**, 26279–26285.
- 12 Y. Liang, P. Xiao, S. Wang, J. Shi, J. He, J. Zhang, Y. Huang and T. Chen, *J. Mater. Chem. C*, 2018, **6**, 6666–6671.
- 13 M. Liu, X. Pu, C. Jiang, T. Liu, X. Huang, L. Chen, C. Du, J. Sun, W. Hu and Z. L. Wang, *Adv. Mater.*, 2017, **29**, 1703700.
- 14 Y. Gao, H. Ota, E. W. Schaler, K. Chen, A. Zhao, W. Gao, H. M. Fahad, Y. Leng, A. Zheng, F. Xiong, C. Zhang, L. C. Tai, P. Zhao, R. S. Fearing and A. Javey, *Adv. Mater.*, 2017, **29**, 1701985.

- 15 I. You, B. Kim, J. Park, K. Koh, S. Shin, S. Jung and U. Jeong, *Adv. Mater.*, 2016, **28**, 6359–6364.
- 16 X. Wang, Y. Zhang, X. Zhang, Z. Huo, X. Li, M. Que, Z. Peng, H. Wang and C. Pan, *Adv. Mater.*, 2018, **30**, 1706738.
- 17 Y. Lee, Y.-J. Park, C. Kim, J.-H. So, B. Yeom and H.-J. Koo, *Polymer*, 2019, **164**, 1–7.
- 18 Y. Yang, J. Liu, J. Cao, Z. Zhou and X. Zhang, *J. Mater. Chem. C*, 2019, **7**, 578–585.
- 19 M. Park, J. Im, M. Shin, Y. Min, J. Park, H. Cho, S. Park, M. B. Shim, S. Jeon, D. Y. Chung, J. Bae, J. Park, U. Jeong and K. Kim, *Nat. Nanotechnol.*, 2012, **7**, 803–809.
- 20 Y. Lin, L. Huang, L. Chen, J. Zhang, L. Shen, Q. Chen and W. Shi, *Sens. Actuators, B*, 2015, **216**, 176–183.
- 21 X. Zhao, F. Chen, Y. Li, H. Lu, N. Zhang and M. Ma, *Nat. Commun.*, 2018, **9**, 3579.
- 22 J. H. Pu, X. J. Zha, M. Zhao, S. Li, R. Y. Bao, Z. Y. Liu, B. H. Xie, M. B. Yang, Z. Guo and W. Yang, *Nanoscale*, 2018, **10**, 2191–2198.
- 23 D. Janczak, M. Sloma, G. Wroblewski, A. Mlozniak and M. Jakubowska, *Sensors*, 2014, **14**, 17304–17312.
- 24 Q. Liu, J. Chen, Y. Li and G. Shi, *ACS Nano*, 2016, **10**, 7901–7906.
- 25 W. Luo, T. Wu, B. Chen, M. Liang and H. Zou, *ACS Appl. Mater. Interfaces*, 2017, **9**, 43239–43249.
- 26 J. Gao, X. Wang, W. Zhai, H. Liu, G. Zheng, K. Dai, L. Mi, C. Liu and C. Shen, *ACS Appl. Mater. Interfaces*, 2018, **10**, 34592–34603.
- 27 S. Cho, J. H. Song, M. Kong, S. Shin, Y. T. Kim, G. Park, C. G. Park, T. J. Shin, J. Myoung and U. Jeong, *ACS Appl. Mater. Interfaces*, 2017, **9**, 44096–44105.
- 28 S. H. Kim, S. Jung, I. S. Yoon, C. Lee, Y. Oh and J. M. Hong, *Adv. Mater.*, 2018, **30**, 1800109.
- 29 B. Nie, X. Li, J. Shao, X. Li, H. Tian, D. Wang, Q. Zhang and B. Lu, *ACS Appl. Mater. Interfaces*, 2017, **9**, 40681–40689.
- 30 Y. Hu, T. Zhao, P. Zhu, Y. Zhu, X. Shuai, X. Liang, R. Sun, D. D. Lu and C.-P. Wong, *J. Mater. Chem. C*, 2016, **4**, 5839–5848.
- 31 J. Kang, D. Son, G. N. Wang, Y. Liu, J. Lopez, Y. Kim, J. Y. Oh, T. Katsumata, J. Mun, Y. Lee, L. Jin, J. B. Tok and Z. Bao, *Adv. Mater.*, 2018, **30**, 1706846.
- 32 S. Lin, Y. Zhong, X. Zhao, T. Sawada, X. Li, W. Lei, M. Wang, T. Serizawa and H. Zhu, *Adv. Mater.*, 2018, **30**, 1803004.
- 33 Q. Zhang, L. Liu, C. Pan, D. Li and G. Gai, *J. Mater. Chem. C*, 2018, **6**, 1746–1752.
- 34 C. S. Boland, U. Khan, G. Ryan, S. Barwich, R. Charifou, A. Harvey, C. Backes, Z. Li, M. S. Ferreira and M. E. Möbius, *Science*, 2016, **354**, 1257–1260.
- 35 J. Hou, M. Liu, H. Zhang, Y. Song, X. Jiang, A. Yu, L. Jiang and B. Su, *J. Mater. Chem. A*, 2017, **5**, 13138–13144.
- 36 X. Zhong, H. Hu and H. Fu, *ACS Appl. Mater. Interfaces*, 2018, **10**, 25697–25705.
- 37 C. Xu, Y. Wang, J. Wu, S. Song, S. Cao, S. Xuan, W. Jiang and X. Gong, *Compos. Sci. Technol.*, 2017, **153**, 168–177.
- 38 K. Liu, A. Pei, H. R. Lee, B. Kong, N. Liu, D. Lin, Y. Liu, C. Liu, P. C. Hsu, Z. Bao and Y. Cui, *J. Am. Chem. Soc.*, 2017, **139**, 4815–4820.
- 39 J. Liang and X. H. Zhang, *J. Mater. Civ. Eng.*, 2014, **27**, 04014250.
- 40 R. Martin, A. Rekondo, A. R. de Luzuriaga, A. Santamaria and I. Odriozola, *RSC Adv.*, 2015, **5**, 17514–17518.
- 41 S. S. Zhang, S. Wang, Y. P. Wang, X. W. Fan, L. Ding, S. H. Xuan and X. L. Gong, *Composites, Part A*, 2018, **112**, 197–206.
- 42 Z. H. Tan, W. H. Li and W. Huang, *Smart Mater. Struct.*, 2018, **27**, 075048.
- 43 T. Wu and B. Chen, *ACS Appl. Mater. Interfaces*, 2016, **8**, 24071–24078.
- 44 R. Cross, *Am. J. Phys.*, 2012, **80**, 870–875.
- 45 A. Lekawa-Raus, K. K. K. Koziol and A. H. Windle, *ACS Nano*, 2014, **8**, 11214–11224.
- 46 S. Chun, W. Son, H. Kim, S. K. Lim, C. Pang and C. Choi, *Nano Lett.*, 2019, **19**, 3305–3312.
- 47 C. Lucarotti, C. M. Oddo, N. Vitiello and M. C. Carrozza, *Sensors*, 2013, **13**, 1435–1466.
- 48 L. Wang and Y. Han, *Composites, Part A*, 2013, **47**, 63–71.
- 49 L. Wang, F. Ma, Q. Shi, H. Liu and X. Wang, *Sens. Actuators, A*, 2011, **165**, 207–215.
- 50 Q. Zheng, J. F. Zhou and Y. H. Song, *J. Mater. Res.*, 2011, **19**, 2625–2634.
- 51 X. W. Zhang, Y. Pan, Q. Zheng and X. S. Yi, *J. Polym. Sci., Part B: Polym. Phys.*, 2000, **38**, 2739–2749.